RSC Advances

ROYAL SOCIETY OF CHEMISTRY

www.rsc.org/advances

THERMALLY ENHANCED HIGH PERFORMANCE CELLULOSE NANO FIBRIL BARRIER MEMBRANES

Sudhir Sharma[a], Xiaodan Zhang[b], Sandeep Nair[c], Arthur Ragauskas[c], Junyong Zhu[d], Yulin Deng[a]

[a:] School of Chemical & Biomolecular Engineering and IPST at GT, Georgia Institute of Technology, Atlanta, GA 30332, USA

[b:] School of Materials Engineering, Georgia Institute of Technology, Atlanta, GA 30332, USA

[c:] School of Chemistry and Biochemistry, Georgia Institute of Technology, Atlanta, GA 30332, USA

[d:] USDA Forest Service, Forest Products Laboratory, Madison, WI 53726, USA

ABSTRACT

Reported here is a method of thermal treatment to enhance barrier properties of membranes made from Cellulose Nano Fibrils (CNFs). CNF membranes of 75±5μm thickness were prepared by evaporation of water from a suspension of CNFs. This was followed by thermal treatment at different temperatures (100°C, 125°C, 150°C, and 175°C) for 3 hours and subsequent conditioning at 23°C and 50% relative humidity for 24 hours. Increasing thermal treatment temperature correlated with enhanced barrier properties; the oxygen and water vapor permeability decreased by 25 fold and 2 fold respectively after treatment at 175°C. The reduction in permeability was attributed to increase in crystallinity, reduction of the inter fibril space or porosity, and increase in hydrophobicity. These effects were also demonstrated to be analogous to Hornification of cellulose fibers.

Keywords: Cellulose Nano fibrils (CNFs), packaging, barrier, sustainable, permeability

INTRODUCTION

Packaging materials are used for providing a barrier against oxygen, water, grease microbes, and odor for food, pharmaceuticals, cosmetics, and other dry goods. The most commonly used barrier packaging materials are glass, metals (aluminum and tin), and petroleum based plastics. Paper based barrier packaging is also widely used; however, the paper substrate must be coated by aluminum, wax or petroleum based plastics or polymers to enhance barrier properties that the paper substrate lacks. These materials have various disadvantages: they are unsustainable, fragile, increase cost of transportation and are non-renewable[1-5]. Cellophane is the only cellulose based material currently used for barrier packaging. However, the production of cellophane is via a viscose route which uses reagents and produces byproducts (CS_2 and H_2S respectively) that are harmful to the environment[6-9].

Membranes made from CNFs have garnered much attention as barrier materials due to their mechanical and gas barrier properties being comparable to synthetic polymeric materials currently used[1, 4, 8, 10-16]. Moreover, they are renewable and biodegradable. Even though pure CNF films have shown good gas barrier properties under dry conditions, these barrier properties tend to degrade under humid conditions due to the hydrophilic nature of cellulose[17]. CNFs are cellulose fibrils with diameters between 10-50nm and length up to 1000nm. CNFs show different properties in many aspects than cellulose fibers owing to their smaller size and high aspect ratio.

In order to enhance the barrier and mechanical properties of CNF membranes, researchers have commonly used methods such as coating CNFs with polymers, grafting other polymers onto the CNFs or using a high aspect ratio filler material to obtain a composite membrane[1, 18-21]. The inclusion of high aspect ratio filler materials is a widely used method that avoids chemical modification of the fibers to enhance barrier and mechanical properties[13, 22, 23]. However, this method has the inherent disadvantage that the filler materials might limit recyclability and biodegradability of the resulting composite material. The methods to chemically modify the CNFs have the disadvantage that the use of chemical reagents for

modification is required, which may hurt the case for the resulting composite material being a completely green material. Moreover, these methods may inhibit the internal hydrogen bonding between fibril surface –OH groups responsible for imparting strength to the membranes.

In this study we propose a simple oven heating of the films after drying. This would be akin to controlled Hornification of the CNFs. By controlled Hornification, we imply that the degree of which the films undergo Hornification can be controlled by the time and temperature of heating. Heating the films would help in inducing Hornification, or the closure of pores between the fibers due to bonding between –OH groups on the surface of the fibers, increase in crystallinity due to co crystallization and also reduced affinity for water. This method is expected to provide an alternative route for enhancing barrier properties of CNF membranes over other methods such as chemical modification and addition of filler materials.

EXPERIMENTAL SECTION

CNF Preparation

Elementally chlorine-free (ECF) bleached Kraft pulp from softwood (Loblolly pine) was obtained as a commercial sample. The pulp at 2 % solids was soaked in deionized water for 24 h and then disintegrated using a lab disintegrator (TMI, Ronkonkoma, NY, USA) for 10,000 revolutions. It was then fibrillated for 12 hours using a SuperMassColloider (MKZA6-2, Masuko Sangyo Co., Ltd, Japan) at 1500 rpm. Pulp was fed continuously to the colloider consisting of two ceramic grinding discs positioned on top of each other. This was operated at contact grinding with the gap of the two discs adjusted to -100 μm. Zero gap between discs corresponds to the starting point, where the two discs just start to graze each other before loading pulp. The presence of pulp between the discs ensured that there is no direct contact between the discs even at the negative setting. The 12 hour grinding process through the SuperMassColloider fibrillates the cellulose fibers to CNFs. The transformation of the cellulose fibers to CNFs is shown in figure 1. The CNFs were then treated with Kathon CP/ICP II (Rohm and Haas Company, Bellefonte, PA, USA) at a dose of 10 μl/ml of fibrillated suspension in order to avoid mold growth.

Membrane Preparation

The CNF suspension was diluted to 1% and heated at 100°C while being vigorously stirred. Subsequently the suspension was poured on to a glass dish to air dry. It took 2-3 days for the water to completely evaporate and form a film. Films of 75±5μm in thickness were obtained.

For permeation and water retention measurements, the films were cut into discs of diameter 50mm. The samples for tensile testing were cut into 45mmX12mm size rectangular specimens. Cut outs from the samples were also used for SEM, XRD and TGA analysis. The samples were then heated in an oven at different temperatures (100°C, 125°C, 150°C, and 175°C) for 3 hours each, leaving one set of samples not heated as the reference sample. After the thermal exposure, all samples were allowed to cool to room temperature and stored in a humidity controlled room at 23°C and 50% relative humidity for 24 hours before any measurements were made.

Membrane Characterization

Oxygen Permeability was measured with a constant pressure difference device. The device consists of a membrane holding cell of diameter 47mm (Milipore XX 45 047 00) connected to an oxygen tank, pressure gauges and connected to a digital flow meter with a least count of 0.01ml/min to measure flow rate. This follows standard constant pressure permeability measurement protocol as described by Bhandari et al and Carruthers et al[24, 25]. A digital flow meter instead of a bubble flow meter was used; Oxygen Permeability was calculated as below,

$$OP = \frac{flow.T}{A.\Delta P}\left(\frac{cc.\mu m}{day.m^2.kPa}\right)$$
(1)

Here, the flow was measured by the flow meter in ml/min, T was the thickness of the film (μm), A the area of the film (m^2), and ΔP the pressure drop (in kPa) across the film. Measurements were made in triplicate.

Water Vapor Permeability was measured using a modified version of the ASTM E-96-95 method. Instead of a standard dish, centrifuge tubes were used, and the chamber was maintained at 40°C and vacuum. Water Vapor Permeability was measured as the Water vapor transmission rate multiplied by the thickness of the films, and divided by the pressure difference across the membrane. The Water Vapor Permeation was calculated as below,

$$WVP = \frac{\Delta m.T}{\Delta t.A.\Delta P} \left(\frac{g.\mu m}{day.m^2.kPa} \right) \qquad\qquad (2)$$

Here, Δm is the weight loss of water from the centrifuge tube, and Δt is the time of experiment in seconds. A and ΔP are area (m^2) and pressure drop (kPa), respectively. In this case, the vapor pressure of water outside the film (downstream, in the oven) is assumed to be zero, while inside the centrifuge tube (upstream) is the saturation pressure of water at 40°C. Measurements were made in triplicate.

Water retention value was measured as the increase in weight of the membranes when in contact with water in fully flooded conditions. This was a modification to a standard Cobb test(T441om-90) as described in TAPPI test methods. A 50mm circular sample was placed into a beaker containing 150ml of water. The sample was kept fully submerged in the beaker for 30 minutes. After 30 minutes, the excess water was squeezed out by placing the sample between two sheets of blotting paper and pressing with a Cobb test rolling pin. The difference between the squeezed final wet weight and the initial dry weight of the samples was used to calculate the Water Retention Value. The measurements for each sample were made in triplicate.

Contact angle of water on the membranes was measured using a First Ten Angstrom contact angle analyzer and FTA32 software. 5µm droplets of water were carefully placed on the sample surface using a Hamilton precision syringe[3, 26]. Five measurements were made for each sample.

X ray Diffraction (XRD) analysis was carried out using a PANalytical X Ray diffractometer using a Cu-Kα source (λ = 0.154nm) with a 2θ range from 10 − 26° with a scanning step of 0.033°. Crystallinity was calculated as,

$$\alpha\% = \frac{I_{cr}}{I_{cr}+I_{am}} \: X \: 100 \tag{3}$$

Here I_{cr} and I_{am} were the maximum intensity of the crystalline and amorphous peaks respectively[27, 28]

The average width of crystallites in the 002 lattice planes were evaluated as[27, 28]

$$L_{002} = \frac{K.\lambda}{\beta_\theta.cos\theta} \tag{4}$$

Where K is the Scherrer Constant (0.9), λ is the wavelength of the diffractometer (0.154nm), β is the width of the crystalline peak at half height, and θ is half of the 2θ value at maximum intensity for the crystalline peak.

Thermogravimetric Analysis (TGA) was done using a Perkin Elmer Pyris 2600 TGA instrument. The originally heat treated and conditioned samples were heated from 30°C to 500°C at a rate of 10°C/min. All measurements were made under 20ml/min nitrogen flow.

SEM Images were taken using a LEO 1530, Carl Ziess instrument. Cross section samples were prepared and were coated with gold using a Quorum 150 R ES instrument before imaging. The images were taken at 3kV - 5kV accelerating voltage as necessary.

Mechanical Testing of the material was carried out with an Instron Bluehill 2 instrument. The films were tested with a 10KN load cell and were stretched at a rate of 5mm/min[10, 11].

RESULTS AND DISCUSSION

XRD analysis

XRD analysis showed that the crystalline structure of the membranes was altered significantly with increasing treatment temperature. To determine the values for calculation, individual peaks were fitted with a pseuo – Voight distribution using XRD analysis software. The XRD spectrum (Figure 2) showed a reduction in the intensity of the amorphous region (~15°), whereas the crystalline peaks (~22.5°) became broader with increasing treatment temperature. This is important because, the broadening of the crystalline peak would indicate increasing size

of crystallites, confirming with the co – crystallization mechanism of hornification. Crystallinity of the membranes also increased from 65% to almost 70% after treatment at 175°C. The size of crystallites in the 002 lattice plane calculated from the widths at half maximum of the crystalline peak heights also showed increase from 4nm to 6nm with increasing temperature[27, 28]. The increase in crystallinity and size of crystallites is caused by two mechanisms, co – crystallization of crystalline regions in the CNFs and some degradation of the amorphous regions during thermal exposure[27-29].

Water Retention Value (WRV)

With increasing treatment temperature the contact angle increased while the water retention value decreased. The water retention value decreased by almost 57%, while contact angle increased from 64° to 95° in the samples treated at 175°C as compared to untreated samples, as shown in table 1. Decreasing water retention value correlates directly with reduced porosity between fibrils[27, 28, 30, 31]; whereas, a shrinking more wrinkled surface causes increased contact angle due to an increase in surface roughness[32]. Furthermore, the observation of reduction in porosity and the increase in hydrophobicity inferred from these measurements also point toward an increased degree of internal hydrogen bonding of the fibril surface –OH groups[30, 31].

SEM Characterization

The change in fibril morphology analogous to Hornification of cellulose fibers is evident in the SEM images of both the surface and the cross section of the CNF membranes. In the SEM images of the untreated samples (Figure 3(a) and 3(b)) an open, porous structure can be observed. Whereas, in the SEM images (Figure 3(c) and 3(d)) of samples treated at 175°C, the loss of the inter fibril porous space is observed in both the surface and cross section. In the untreated samples, the fibrillated structure of the individual fibrils can still be observed, whereas in the treated samples, the fibrils are matted down and packed much more densely. This change in fibril morphology can be explained by the removal of water from the inter fibril

space causing the fibrils to shrink and hydrogen bond with each other via surface –OH groups[27, 30, 33-35].

The SEM images corroborate the two observations of increase in crystallinity and hydrophobicity. Since the three important mechanisms of Hornification; reduction of porosity, increase in hydrophobicity and increase in crystallinity were observed concomitantly in the CNF membranes upon thermal exposure, it can be safely asserted that thermal exposure results in the same effects for membrane made from CNFs as the mechanism for Hornification of cellulose fibers.

TGA Analysis

The TGA curves (Figure 4) show that the characteristic shape of the curves has not changed but the onset and magnitude of weight loss before degradation has reduced significantly. It must be noted that these measurements were made after the membranes had been conditioned for 24 hours at 50% Relative Humidity. Therefore, this points to the reduced hygroscopic property of the membranes, which also agrees with reduction in water retention value. It can also be observed from the derivative TGA curves that the temperature at which maximum rate of degradation is observed has somewhat decreased for the thermally treated membranes, which could mean there is some degradation of the membrane during the thermal treatment. Table 2 shows that the change in thermal properties is gradual with increase in treatment temperature. This is important because the equilibrium water adsorbed acts as a plasticizing agent keeping the membrane soft and elastic. This adsorbed water also acts as a medium for gas permeation through the membrane.

Mechanical

The membranes showed decline in strength with increasing treatment temperature (Table 3). The reduction in strength is due to the decomposition of the amorphous cellulose polymer networks and the increase in the crystalline nature of the material, which causes it to be increasingly brittle[27, 31]. Additionally, it is thought that water acts as a plasticizing agent

enhancing the tensile property of the material. With removal of the water held in the pores of the membranes, the plasticizing effect is reduced and the membranes show loss of strength and increase in brittleness.

Permeability

AS shown in figure 5 Oxygen and water vapor permeability decreased significantly with increasing treatment temperature. In the best case, oxygen permeability declined by almost 25 fold while the water vapor permeability declined to half of the untreated membrane value. The reduction in oxygen and water vapor permeability is due to three reasons. The first two as hypothesized are common reasons, primarily the significant reduction in porosity of the material hinders diffusion; and second, the increase in crystallinity hinders the solubility of the gas and water vapor in the material[8, 17, 36]. The third reason for reduction in water vapor permeability is the increase in hydrophobicity of the material. While the untreated membrane adsorbs water quickly in the presence of a water vapor stream, the thermally treated membranes show a much lower degree of water adsorption. This effect arises from the internal hydrogen bonding of the free –OH groups causing increased hydrophobicity rather than just increase in crystallinity. While this clearly would reduce the water vapor permeability, it also has a significant effect on the oxygen permeability of the membrane.

Since water also acts as a permeation medium for gases, the reduction of water retention helps in reducing overall permeability of the membrane. This effect is demonstrated well in studies where permeation of gases under humid streams is studied, and it is observed that gas barrier deteriorates under humid conditions. However, in this case, it can be easily contended that due to the limited ability of thermally treated CNF membranes to adsorb water, the deterioration of gas barrier properties under humid conditions can be avoided. A similar effect has been noted by Ostberg et al.[10] who used a hot press method to form CNF membranes. Since the membranes formed were quite dense and had some thermal exposure during the drying process they showed reduced degradation of barrier under humid conditions as compared to CNF films prepared from methods not involving any thermal exposure in other studies.

The effects of thermal exposure demonstrated here are in agreement with past studies demonstrating the effects of thermal exposure on cellulose fibers. Past studies have demonstrated that the loss of porosity occurs due to the removal of water from between the pores of the cellulose fibers which causes the fibers to shrink. Researchers have used solute exclusion, low temperature nitrogen adsorption, 1H and 2H NMR relaxation to determine the changes in pore structure during the drying process[27, 30, 33-35]. In all studies it was demonstrated that increasing thermal exposure caused reduction in porosity. The concomitant increase in crystallinity has also been studied by various methods including XRD analysis, 1H, 2H, Carbon 13 NMR, and FTIR methods[27-29, 31]. In most cases it was shown that the crystallinity increased due to the co – crystallization of the crystalline regions. Some authors have also contended that the increase in crystallinity is due to amorphous regions being converted to crystalline during the drying process.

The hornified fibers not only become less porous and more crystalline but also increasingly hydrophobic during the drying process. The increase in hydrophobicity is indicated by increase in water contact angle and reduction of water retention value. The reduction of water retention value of fibers is mainly attributed to the formation of irreversible of hydrogen bonds between free – OH groups on the cellulose fibrils. This hydrogen bonding is also related to the changes in morphology, and the fibrils are observed to shrink and suffer a loss in porosity upon drying. We also observed that the surface became increasingly wrinkled and had increased surface roughness, which could be the cause of increased contact angle. This is an agreement with past studies relating surface roughness to hydrophobicity and contact angle. Studies of effect of time and temperature on the degree of Hornification have demonstrated that both parameters play an important role. Here, the drying of the membranes at different temperatures would have caused different drying rates and at higher drying temperatures, there has been observed a higher degree of loss of porosity and reduction in water retention values as a consequence.

CONCLUSIONS

In this study the effects of thermal exposure on CNF membranes analogous to Hornification to improve barrier properties were demonstrated. The effects were observed on a bulk level in the membranes and also on a fibril level. This method avoids the usage of any filler materials or chemical reagents. The XRD analysis determined that both size of crystallites and the crystallinity of the material increased with increasing treatment temperature. Water retention value decreased significantly while surface contact angle increased from hydrophilic to hydrophobic pointing towards an increase in surface roughness, fiber shrinkage, internal hydrogen bonding between the fibrils and loss of porosity. SEM images concurred with the XRD and water retention measurements in making evident that the fibrils underwent shrinking and loss of inter fibril porosity. Finally, both oxygen permeability and water vapor permeability decreased significantly upon thermal treatment due to mechanisms analogous to Hornification of cellulose fibers. The reduction was ascribed to hindered diffusion due to a more dense structure and reduced gas solubility due to increased crystallinity. The significant decrease in water vapor permeability was also thought to be due to the significant increase in hydrophobicity of the membranes. Even though loss of mechanical strength of the materials due to an increase in crystallinity and brittleness was observed, the enhancement of barrier properties is significant.

Hereby, we have demonstrated that controlled thermal exposure can serve as a good method for enhancing the barrier properties of CNF membranes without using external chemical agents and maintaining the native cellulose material as a green, recyclable and biodegradable material. The study also paves the path for further tuning of CNF membrane properties via controlled thermal exposure.

AUTHOR INFORMATION

Corresponding Author *E-mail: yulin.deng@ipst.gatech.edu, Tel: +01 404 894 5759; Fax +01 404 894 4778

RSC Advances Accepted Manuscript

Notes
The authors declare no competing financial interest.

FIGURE and TABLE CAPTIONS

Figure 1.(a) Cellulose Fibers before fibrillation. (b) Cellulose fibers after 12 hours of fibrillation through SuperMassColloider

Figure 2. XRD Analysis

Figure 3. Surface Morphology (a) Untreated Samples. (b) Cross Section Untreated Samples. (c) Surface Morphology, Samples treated at 175°C. (d) Cross Section, Samples treated at 175°C.

Figure 4. Thermo Gravimetric Analysis

Figure 5. Oxygen and Water Vapor Permeability

Table 1. WRV and Contact Angle Measurement

Table 2. Onset and Max Weight Loss before degradation

Table 3: Ultimate Tensile Strength

Figures and Tables

Attached in separate file

References

1.   I. S. Bayer, D. Fragouli, A. Attanasio, B. Sorce, G. Bertoni, R. Brescia, R. Di Corato, T. Pellegrino, M. Kalyva, S. Sabella, P. P. Pompa, R. Cingolani and A. Athanassiou, *ACS Appl Mater Interfaces*, 2011, 3, 4024-4031.
2.   G. Findenig, S. Leimgruber, R. Kargl, S. Spirk, K. Stana-Kleinschek and V. Ribitsch, *ACS Applied Materials & Interfaces*, 2012, 4, 3199-3206.
3.   L. Li, V. Breedveld and D. W. Hess, *ACS Applied Materials & Interfaces*, 2013, 5, 5381-5386.
4.   K. Syverud and P. Stenius, *Cellulose*, 2009, 16, 75-85.
5.   V. Siracusa, *International Journal of Polymer Science*, 2012, 2012, 11.
6.   M. I. Vázquez, C. Milano, R. de Lara, O. Guerrero, C. Herrera and J. Benavente, *Desalination*, 2006, 200, 15-17.
7.   Y. Kamiya and F. Takahashi, *Journal of Applied Polymer Science*, 1977, 21, 1945-1954.
8.   J. Wu and Q. Yuan, *Journal of Membrane Science*, 2002, 204, 185-194.

9. W. L. Hyden, *Industrial & Engineering Chemistry*, 1929, 21, 405-410.
10. M. Österberg, J. Vartiainen, J. Lucenius, U. Hippi, J. Seppälä, R. Serimaa and J. Laine, *ACS Applied Materials & Interfaces*, 2013.
11. C.-N. Wu, T. Saito, S. Fujisawa, H. Fukuzumi and A. Isogai, *Biomacromolecules*, 2012, 13, 1927-1932.
12. H. Sehaqui, Q. Zhou, O. Ikkala and L. A. Berglund, *Biomacromolecules*, 2011, 12, 3638-3644.
13. N. D. Luong, N. Pahimanolis, U. Hippi, J. T. Korhonen, J. Ruokolainen, L.-S. Johansson, J.-D. Nam and J. Seppala, *Journal of Materials Chemistry*, 2011, 21, 13991-13998.
14. S. Belbekhouche, J. Bras, G. Siqueira, C. Chappey, L. Lebrun, B. Khelifi, S. Marais and A. Dufresne, *Carbohydrate Polymers*, 2011, 83, 1740-1748.
15. M. Minelli, M. G. Baschetti, F. Doghieri, M. Ankerfors, T. Lindström, I. Siró and D. Plackett, *Journal of Membrane Science*, 2010, 358, 67-75.
16. M. Henriksson, L. A. Berglund, P. Isaksson, T. Lindström and T. Nishino, *Biomacromolecules*, 2008, 9, 1579-1585.
17. C. Aulin, M. Gällstedt and T. Lindström, *Cellulose*, 2010, 17, 559-574.
18. D. Stanssens, H. Van den Abbeele, L. Vonck, G. Schoukens, M. Deconinck and P. Samyn, *Materials Letters*, 2011, 65, 1781-1784.
19. S. Cao, D. Song, Y. Deng and A. Ragauskas, *Industrial & Engineering Chemistry Research*, 2011, 50, 5628-5633.
20. V. Bhardwaj, A. Macintosh, I. D. Sharpe, S. A. Gordeyev and S. J. Shilton, *Annals of the New York Academy of Sciences*, 2003, 984, 318-328.
21. X. Samain, V. Langlois, E. Renard and G. Lorang, *Journal of Applied Polymer Science*, 2011, 121, 1183-1192.
22. G. W. Jeon, J.-E. An and Y. G. Jeong, *Composites Part B: Engineering*, 2012, 43, 3412-3418.
23. H. Kim, Y. Miura and C. W. Macosko, *Chemistry of Materials*, 2010, 22, 3441-3450.
24. D. Bhandari, K. O. Olanrewaju, N. Bessho, V. Breedveld and W. J. Koros, *Separation and Purification Technology*, 2013, 104, 68-80.
25. S. B. Carruthers, G. L. Ramos and W. J. Koros, *Journal of Applied Polymer Science*, 2003, 90, 399-411.
26. B. Balu, V. Breedveld and D. W. Hess, *Langmuir*, 2008, 24, 4785-4790.
27. Y.-m. Chen, J.-q. Wan, M.-z. Huang, Y.-w. Ma, Y. Wang, H.-l. Lv and J. Yang, *Carbohydrate Polymers*, 2011, 85, 759-764.
28. Y. Chen, Y. Wang, J. Wan and Y. Ma, *Cellulose*, 2010, 17, 329-338.
29. Y. Liu, D. Thibodeaux, G. Gamble, P. Bauer and D. VanDerveer, *Applied Spectroscopy*, 2012, 66, 983-986.
30. Å. Östlund, T. Köhnke, L. Nordstierna and M. Nydén, *Cellulose*, 2010, 17, 321-328.
31. M. G. A. Vieira and S. C. S. Rocha, *Chemical Engineering and Processing: Process Intensification*, 2007, 46, 955-963.
32. A. Brancato, F. L. Walsh, R. Sabo and S. Banerjee, *Industrial & Engineering Chemistry Research*, 2007, 46, 9103-9106.
33. S. Park, R. A. Venditti, H. Jameel and J. J. Pawlak, *Carbohydrate Polymers*, 2006, 66, 97-103.
34. D. Topgaard and O. Söderman, *Cellulose*, 2002, 9, 139-147.
35. R. C. Weatherwax, *Journal of Colloid and Interface Science*, 1977, 62, 432-446.
36. K. L. Spence, R. A. Venditti, O. J. Rojas, J. J. Pawlak and M. A. Hubbe, *BioResources*, 2011, 6, 4370-4388.
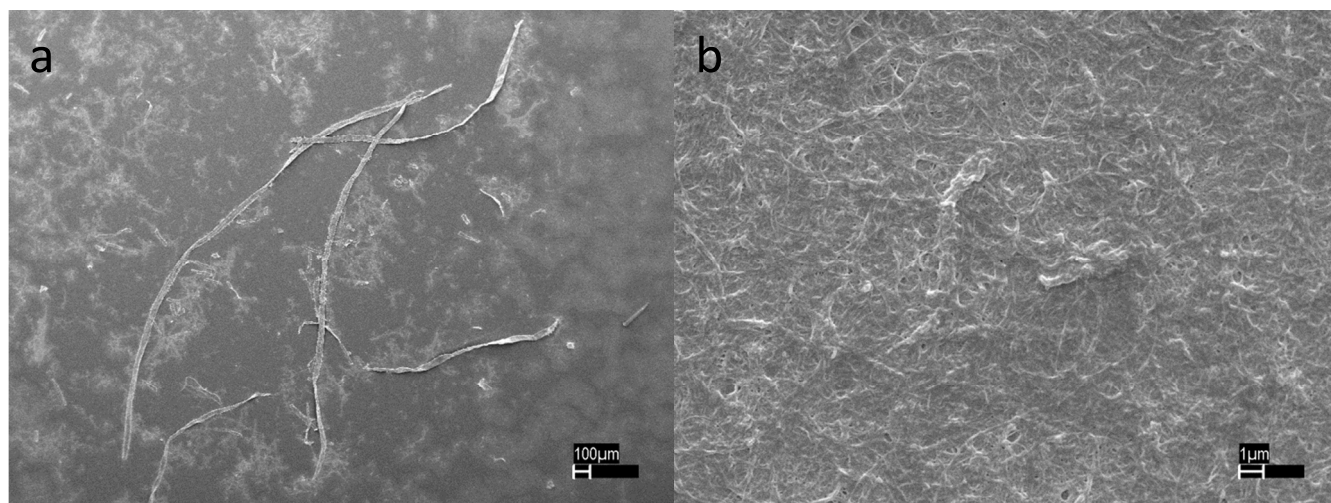
Figure 1: a. Cellulose Fibers before Fibrillation b. Cellulose Fibers after 12 hours of fibrillation through SuperMassColloider
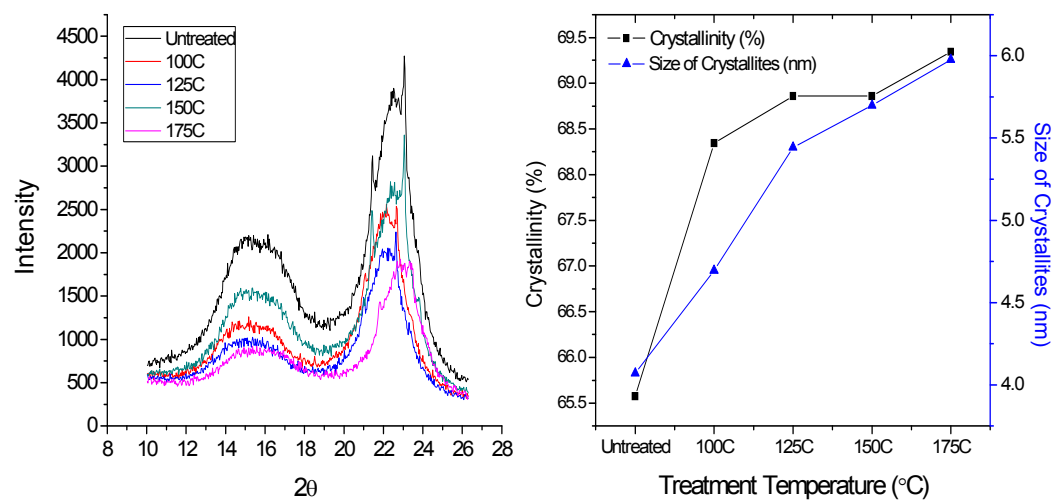
Figure 2: XRD Analysis
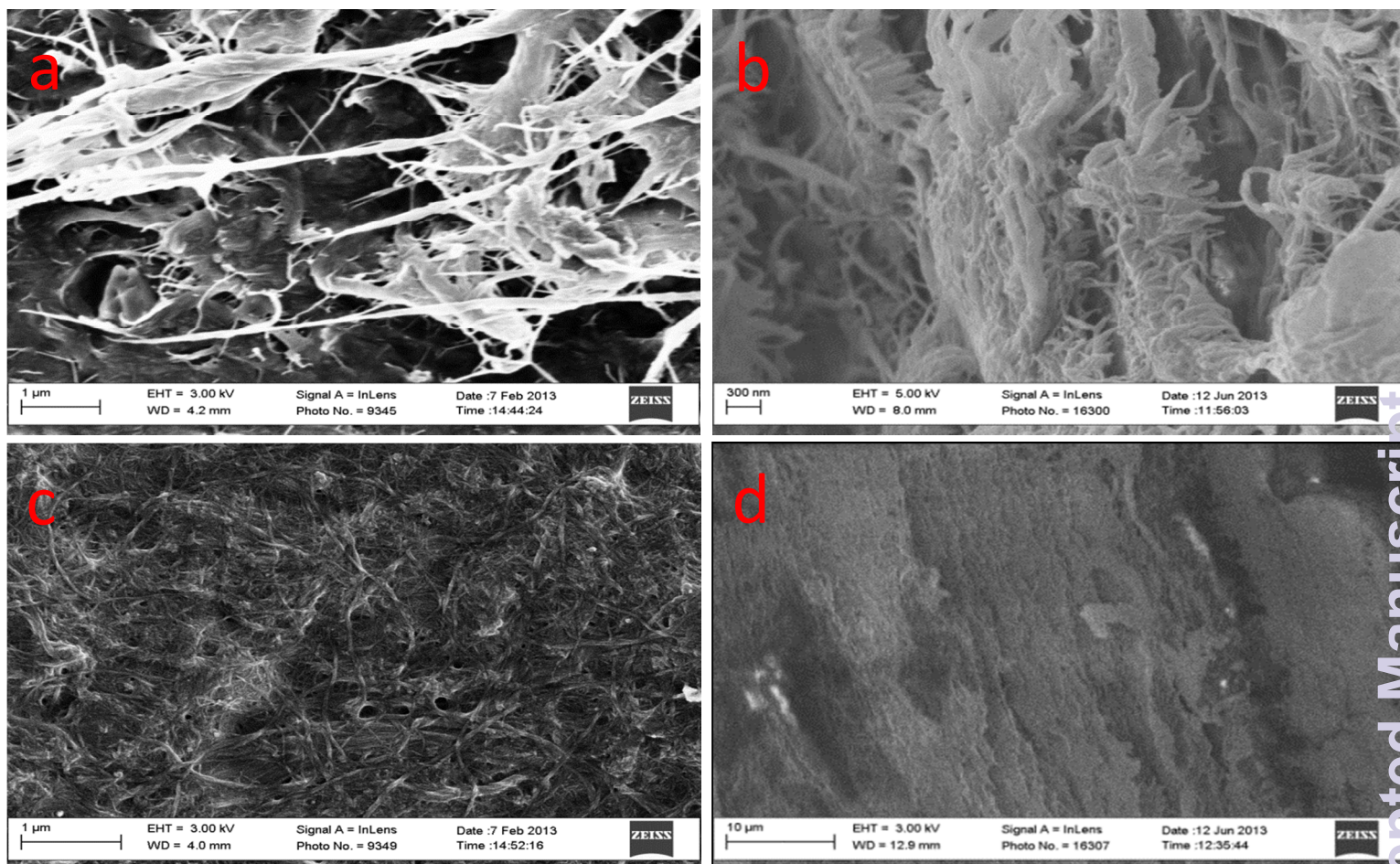
Figure 3: Surface Morphology (a) Untreated Samples. (b) Cross Section Untreated Samples. (c) Surface Morphology, Samples treated at 175°C. (d) Cross Section, Samples treated at 175°C.
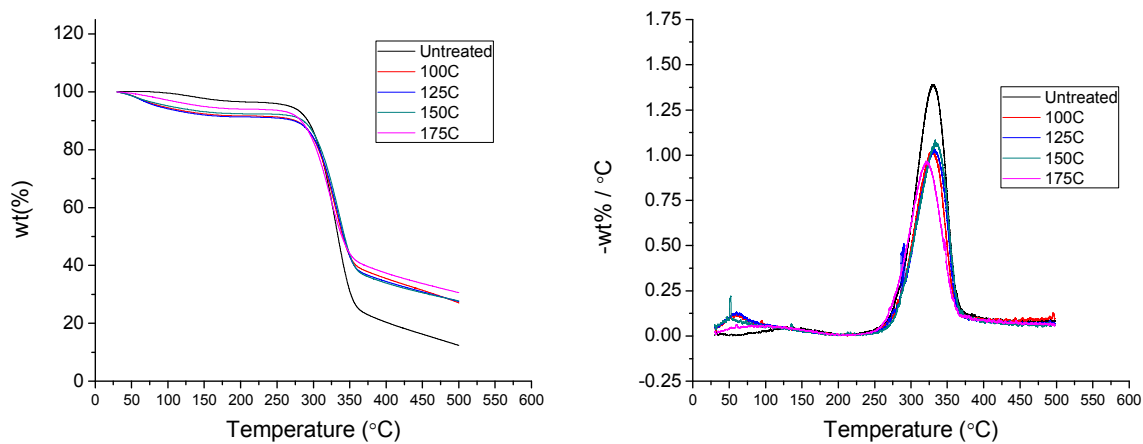
Figure 4: Thermo Gravimetric Analysis
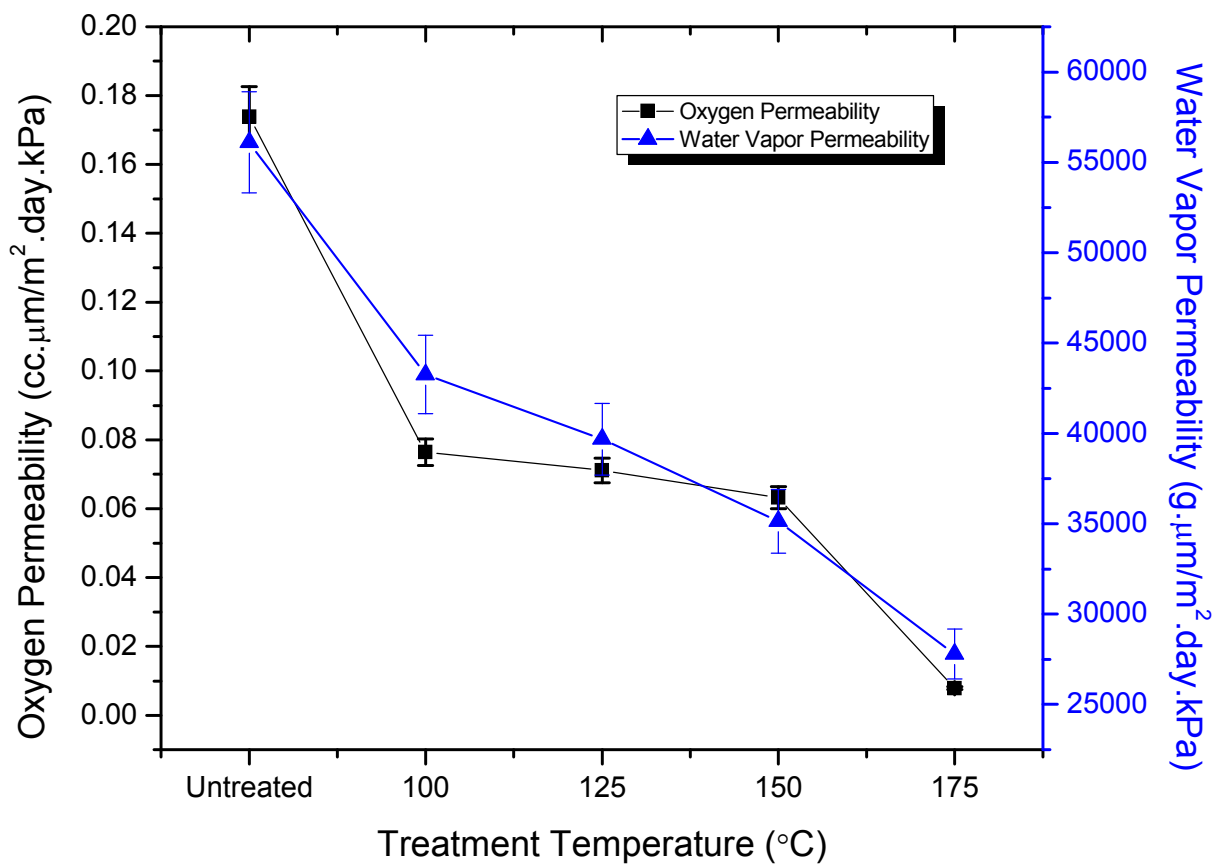
Figure 5: Oxygen and Water Vapor Permeability

Sample	Untreated	100°C	125°C	150°C	175°C
WRV (g/m^2)	126.8±6.3	113.4±5.2	97.2±5.4	76.3±3.8	53.6±2.7
Contact Angle (°)	61.2±3.1	62.7±3.1	81.6±4.1	89.3±4.4	95.2±4.7

Table 1: WRV and Contact Angle

Sample	Untreated	100°C	125°C	150°C	175°C
Max Weight Loss %	71.8	55.09	52.55	51.57	49
Onset Temperature (°C)	288.5	280	271	260	245

Table 2: Onset Temperature and Maximum Weight loss before degradation

Sample	Untreated	100°C	125°C	150°C	175°C
UTS (GPa)	1.14±0.06	1.2±0.06	1.1±0.05	0.9±0.04	0.77±0.04

Table 3: Ultimate Tensile Strength

Graphical Abstract

Extremely high barrier film for oxygen and water moisture permission was obtained by 100% of sustainable cellulose nanofibrils (CNF) with simple heat treatment